APPLICATION OF A FRF BASED MODEL UPDATING TECHNIQUE FOR THE VALIDATION OF FINITE ELEMENT MODELS OF COMPONENTS OF THE AUTOMOTIVE INDUSTRY.

Stefan Lammens, Marc Brughmans and Jan Leuridan

LMS International
Interleuvenlaan 68, B-3001 Leuven, Belgium

Paul Sas

Katholieke Universiteit Leuven
Celestijnenlaan 300B, B-3001 Leuven, Belgium

ABSTRACT.

This paper presents two applications of the RADSER model updating technique (ref. 1). The RADSER technique updates finite element model parameters by solution of a linearised set of equations that optimise the Reduced Analytical Dynamic Stiffness matrix based on Experimental Receptances.

The first application deals with the identification of the dynamice characteristics of rubber mounts.

The second application validates a coarse finite element model of a subframe of a Volvo 480.

INTRODUCTION.

In the design and optimisation of vehicles, numerical models for the prediction of the noise and vibration behaviour play an important role. The validity and reliability of these models can be drastically improved by application of so called 'model updating' techniques. Model updating aims at the verification and correction of numerical models of dynamic structures by means of comparison with experimentally obtained data about the noise and vibration behaviour of the real structure.

This paper discusses the application of a FRF based model updating technique in two different case studies with components of the automotive industry.

The presented updating technique corrects finite element models based on experimentally obtained receptances. The values of a selection of element or material properties of the numerical model are updated in an iterative procedure that matches the numerical receptances with the experimental ones for a selection of frequency points.

The first case study identifies the axial stiffness and damping value of rubber mounts. This rather academic case study shows the use of the presented updating technique for determination of an appropriate damping approach for the description of the mounts in a finite element model. Application of damping in a finite element model is most often a rather cumbersome problem.

The second case study validates a very coarse finite element model of a subframe of a car. Starting from somewhat noisy measurements and via selections of updating parameters and updating frequencies based on simple rules of thumb and common sense, the updating process gives reliability to a coarse, and thus cheap, finite element model.

THE RADSER UPDATING METHOD.

This section shortly explains the RADSER updating method. A detailed discussion can be found in ref. 1.

Mixed static-dynamic reduction.

The following technique is used for reduction of the analytical dynamic stiffness matrix.

The full set of analytical degrees of freedom is partitioned in three groups:

- the active degrees of freedom,
- the 'statically deleted' degrees of freedom,
- the 'dynamically deleted' degrees of freedom.

The statically deleted degrees of freedom are a set of degrees of freedom that can be eliminated from the system matrices by static reduction without a major loss of accuracy. Rotational degrees of freedom for a 3D-beam structure are for instance well suited to be statically deleted degrees of freedom. The dynamically deleted degrees of freedom are all deleted degrees of freedom that cannot be eliminated by means of static reduction without introducing unacceptable inaccuracies in the system matrices. With this partition following reduction scheme can be used to compute the reduced dynamic stiffness matrices needed in the RADSER updating method:

1. Compute the full mass and stiffness matrices.

2. Reduce these matrices with the static reduction method to the combined set of active and dynamically deleted degrees of freedom.

3. Assemble the statically reduced dynamic stiffness matrix.

4. For each updating frequency, reduce the statically reduced dynamic stiffness matrix with the exact dynamic reduction method to the set of active degrees of freedom.

This simple scheme reduces the required computational effort substantially and hardly influences the accuracy of the eventual reduced dynamic stiffness matrix.

Minimisation of the indirect receptance difference.

Consider a set of updating frequencies $\{\omega_i\}$ and a set of updating parameters $\{u\}$. For each ω_i the dynamic stiffness matrix is created from the analytical mass, stiffness and (viscous or structural) damping matrix:

$$[Z_i] = [K] + j \cdot \omega_i \cdot [C] - \omega_i^2 \cdot [M] \tag{1}$$

The above explained reduction scheme yields the reduced dynamic stiffness matrix $\left[Z_i^R\right]$.

For each ω_i the residual forces $\{\varepsilon_i\}$ are written as a function of the updating parameters:

$$\{\varepsilon_i\} = \left[Z_i^R(\{u\})\right] \cdot \left\{H_i^X\right\}_j - \{1\}_j \tag{2}$$

or

$$\{\varepsilon_i\} = \left(\left[Z_i^R\left(\{u^o\}\right)\right] + \left[\Delta Z_i^R\left(\{\Delta u\}\right)\right]\right) \cdot \left\{H_i^X\right\}_j - \{1\}_j \tag{3}$$

where:

$\left\{H_i^X\right\}_j$: experimental FRF with ref. j at freq. ω_i

$\{1\}_j$: vector, component j = 1, all other comp. = 0

$\{u^o\}$: original values of the updating parameters

Using a first order Taylor expansion for $\left[\Delta Z_i^R\left(\{\Delta u\}\right)\right]$ yields:

$$\{\varepsilon_i\} = \left(\left[Z_i^R\left(\{u^o\}\right)\right] + \sum_t \frac{\partial Z_i^R}{\partial u_t} \cdot \Delta u_t\right) \cdot \left\{H_i^X\right\}_j - \{1\}_j \tag{4}$$

or

$$\{\varepsilon_i\} = \sum_t \left(\frac{\partial Z_i^R}{\partial u_t} \cdot u_t^o \cdot \left\{H_i^X\right\}_j \cdot \frac{\Delta u_t}{u_t^o}\right) + \left[Z_i^R\left(\{u^o\}\right)\right] \cdot \left\{H_i^X\right\}_j - \{1\}_j \tag{5}$$

Considering the noise on the measurements, equation (5) is ill conditioned. Premultiplying this equation by the inverse of the dynamic stiffness matrix yields a better conditioned equation:

$$\left\{\varepsilon_i^*\right\} = \sum_t \left(\left[H_i^A\right] \cdot \frac{\partial Z_i^R}{\partial u_t} \cdot u_t^o \cdot \left\{H_i^X\right\}_j \cdot \frac{\Delta u_t}{u_t^o} \right) + \left\{H_i^X\right\}_j - \left\{H_i^A\right\}_j \tag{6}$$

$$\text{where: } \left[H_i^A\right] = \left[Z_i^R\left(\left\{u^o\right\}\right)\right]^{-1} \tag{7}$$

The left hand side of (6) is called the indirect receptance residue.

The combination of the indirect receptance residue for all updating frequencies ω_i results in a linearised minimisation problem:

$$\min\left\|\{\varepsilon\}\right\| \qquad \{\varepsilon\} = \begin{Bmatrix} \vdots \\ \{\varepsilon_i\} \\ \vdots \end{Bmatrix} \tag{8}$$

This linearised minimisation problem is solved iteratively with a least squares approach.

IDENTIFICATION OF MOUNTS.

This case study shows the use of the RADSER model updating technique for the identification of localised damping characteristics. It is a simple and very specific case study. The subject of the case study is the determination of the axial damping and stiffness characteristics of three rubber mounts.

Figure 1 shows the set up. An equilateral steel triangle is connected to a large steel mass through three equal mounts. The mounts are put symmetric with respect to the center of the triangle. In the frequency range of interest, 0 to 150 Hz, the triangle can be seen as a rigid body. Only motion in the z-direction, the axial direction of the mounts, is considered. This configuration is used to determine the axial damping and stiffness characteristics of the mounts using the RADSER model updating technique. The structure was measured experimentally and a finite element analysis was performed.

Experimental set up.

Figure 2 shows the experimental set up. Four accelerometers, PCB Structcel 330A, are placed on the triangle; one in the center (upside down at the bottom side of the triangle) and the three other each in the middle between two mounts. In the center of the triangle a force cel, PCB 208B, is connected. Via the force cel, the excitation force is applied on the structure. The force is generated by a LDS V406 shaker. The test set up is very specific and selectif. Great care was taken to obtain clean and accurate measurements. Everything is focused on the identification of the axial damping and stiffness of the mounts. The configuration is chosen such that residual effects of flexibilities of the mounts in other directions than the axial direction are excluded from the test as much as possible. The only motion that can be excited and measured is a displacement of the triangle as a rigid body in the z-direction with possibly rotations about the x- and y-axis, but without any translation in the x- or y-direction and without any rotation about the z-axis. For small displacements, the mounts are thus only loaded in their axial direction. Table 1 gives an overview of some aquisition parameters.

Figure 3 shows superimposed the four receptances that were measured. They are almost identical. Since the mounts are identical and they are put symmetric with respect to the center of the equilateral triangle and since the triangle was excited at its center, a pure z-translation of the triangle is measured.

Analytical model.

An analytical model of the structure was made. In the model, three different stiffnesses and three different values for the damping characteristics of the mounts are applied. The purpose of the study is to show that with the presented updating technique the different stiffnesses and the different damping values converge to respectively one single stiffness value and one single damping value, i.e. the actual stiffness and damping value of the mounts in the axial direction.

Figure 4 shows the finite element model. The model consists of 57 degrees of freedom (translation in z-direction and rotation about x- and y-axis in 19 nodes). For the triangle, shell elements were used and for the mounts uniaxial spring-damper elements. For the description of the damping behaviour, two different approaches are tried out. A first model describes the mounts as viscous dampers. A second model uses a structural damping approach for the mounts. For the viscous mounts, following element matrix was used:

$$j\omega\begin{bmatrix} c & 0 \\ 0 & c \end{bmatrix}+\begin{bmatrix} k & 0 \\ 0 & k \end{bmatrix} \tag{9}$$

where:

c : axial viscous damping value of the mount,

k : axial stiffness of the mount.

The structural damping mounts use following element matrix:

$$(1+j\eta)\begin{bmatrix} k & 0 \\ 0 & k \end{bmatrix} \tag{10}$$

where:

η : structural damping factor.

Table 2 shows the original values of the stiffness and damping parameters applied in the finite element model.

These stiffness and damping parameters are selected as the updating parameters in the model updating process. This procedure aims at the identification of their actual value. In order to be physically meaningful, they should converge to one value for the stiffnesses and one value for the damping parameters.

Model updating.

Since the experimental data consists of only four degrees of freedom, a reduction of the analytical model is necessary. The mixed static dynamic reduction technique, discussed above, is used. The rotational degrees of freedom (38 out of 57 degrees of freedom) were chosen as statically deleted degrees of freedom. The active degrees of freedom are by definition the four degrees of freedom that correspond to the measured degrees of freedom (translation in z-direction of point 1, 2, 3 and 4). All other translational degrees of freedom (15 out of 19 not statically deleted degrees of freedom) are the dynamically deleted degrees of freedom.

Figure 5 and 6 show superimposed the analytical receptances at the active degrees of freedom.

The updating frequencies are selected as indicated in figure 7. An equal distribution of nine updating frequencies in the range from 40 to 80 Hz was chosen.

Ten updating iterations are run for both models.

Figures 8 and 9 show the updated receptances for the viscous damping model. They coincide quite well with the experimental receptances. Figure 10 gives the convergence of the updating parameters. The stiffnesses converge to about 2.4 10^6 N/m. The viscous damping parameters converge to about 100 Ns/m. Although the three damping parameters and the three stiffness parameters are not perfectly identical, the differences are acceptably small. The obtained damping and stiffness characteristics of the mounts can be further used with reasonable confidence.

For the structural damping model, the results (figure 11 to 13) are even better. The experimental and analytical receptances coincide almost perfectly. Structural damping shows to be a slightly more appropriate damping approach than viscous damping for the description of the axial damping behaviour of the mounts. The stiffness parameters converge to the same value that was found with the viscous model: about 2.4 10^6 N/m. The structural damping parameters converge to about 0.17. Again, the differences are acceptably small and the obtained parameters can be used with reasonable confidence.

Conclusion.

This section showed a succesful application of the RADSER updating technique for the identification of localised damping parameters. The axial stiffness and damping characteristics of rubber mounts were determined through FRF measurements in a selective configuration. Both viscous damping and structural damping were used. The structural damping approach shows to be somewhat more appropriate for the rubber mounts. Both damping approaches generate more than appropriate results.

However simple, this case study showed that the RADSER updating technique is valid for the identification of damping parameters when an accurate and manageable damping approach is provided.

MODEL UPDATING OF A VOLVO 480 SUBFRAME.

The subject of this case study is a subframe of a Volvo 480 automobile. Figure 14 shows the subframe in a set up for an experimental modal analysis test. In a Volvo 480, the subframe supports the engine, the steering house and the lower front wheel carriers. The subframe is connected to the car body via rubber mounts in its four corner points. The purpose of this case study is the updating of a highly idealised finite element model of the subframe with the RADSER model updating technique.

In the development of a finite element model, there is always the trade-off between accuracy and computation cost. Fine meshes of elements generally generate more accurate results than coarse meshes. Coarse meshes need a high degree of idealisation. They can only be used for a global, general prediction of the behaviour of the structure. The use of coarse meshes, however, drastically reduces the computation cost. For components of larger structures, like for instance the Volvo 480 subframe, a rough dynamic prediction is in most cases sufficient, as long as the prediction is reasonably reliable. Fine and detailed finite element models are often too expensive for this purpose. This case study shows the use of the RADSER model updating technique for the verification and correction of a very coarse finite element model of the Volvo 480 subframe. The aim is to obtain a cheap, i.e. with a low number of degrees of freedom, but reliable finite element model.

This section first discusses the acquisition of the experimental FRF's. Next, it describes the original finite element model of the subframe. A correlation study shows the need for model updating. Finally, the updating of the coarse finite element model is discussed.

Acquisition of the experimental FRF's.

Figure 14 shows the experimental set up. The subframe is measured in a free-free configuration. Three soft springs support the structure. Responses are measured triaxially in 37 points with PCB 330A Structcel accelerometers. Figure 15 shows the measurement geometry. The structure is excited in two locations: point 316 in

the z-direction (figure 16) and point 408 in the (-y)-direction (figure 17). Force cells PCB 208B measure the input forces that are generated by B&K Type 4809 shakers. The frequency range of interest is from 0 to about 300 Hz. This range covers the lower, global modes. Table 3 shows the used acquisition and signal processing parameters.

Figure 18 checks the reciprocity. The reciprocity is not perfect. Especially in the ranges before and between the first four resonance peaks, differences are found. In general, the receptances are rather noisy in the ranges between the resonance peaks. Close to the resonances, the receptances are believed to be more accurate.

A modal analysis is performed with the measured FRF's. By means of the Least Squares Complex Exponential (LSCE) technique, implemented in the LMS Cada-X Modal Analysis software (ref. 2), 6 normal modes are identified in the frequency range of interest. Table 4 gives an overview of the experimental modal parameters.

The identification of the sixth mode is somewhat problematical, since both input points of the FRF measurements are rather close to a node of the mode shape. As a consequence, hardly any energy was put into this mode during the measurements. This is reflected by the mode participation factors that are given in table 5. The table shows that also the fifth mode was excited rather poorly. This mode was almost exclusively excited through input point 316. As a consequence, the weighted mode complexity of this mode with respect to input point 408 is poor. Table 6 gives the MAC-values for the experimental mode shapes. From point of view of the MAC-values, the experimental modal model seems to be valid. In the updating process, the experimental mode shapes are not used as reference data. From the experimental modal model only the resonance frequencies are used. The experimental mode shapes are not used but to evaluate the correlation between the experimental data and the analytical model via MAC-values. So, for the fifth and sixth mode shape, these MAC-values must be interpreted with some reserve.

Together with the resonance frequencies, the measured receptances are the reference data for the model updating process. Two sets of 111 receptances (37 response points, triaxial, 2 inputs) are available. In spite of some noisy ranges, the accuracy of the receptances is acceptable. The first four modes are well covered by these receptances. The fifth and a fortiori the sixth mode are not too well represented in the measured receptances.

Finite element model.

A very coarse finite element model of the subframe is developed with MSC/NASTRAN (ref. 3) The measurement geometry (figure 15) is the base for the model. Almost all nodes of the model coincide with an experimental measurement point. Figure 19 shows the model. All elements are CBEAM elements. The CBEAM element is a more or less appropriate element for most of the structure.

The quadrangles 303-304-316-305 and 403-404-416-405 and the triangles 305-306-314, 405-406-414, 308-309-315 and 408-409-415 however are not beam like structures. For these parts, the use of beam elements is not more than an approximate mathematical description of the dynamic behaviour. A sort of shell element seems to be more appropriate at the first sight. However, a fine mesh of shell elements would be necessary to model these parts in a decent way. Beam elements are defined by much more parameters than shell elements. In that way they are, purely mathematically, more flexible to be fitted in a prescribed behaviour. That is why beam elements were chosen instead of shell elements. For an equal number of degrees of freedom, they offer more flexibility in the updating process. The triangles 305-306-314, 405-406-414, 308-309-315 and 408-409-415 are not very important for the global behaviour of the subframe in the configuration of the experimental test. The quadrangles 303-304-316-305 and 403-404-416-405 on the contrary are important for the global dynamic behaviour. Moreover, point 316 is the reference in the first set of experimental receptances. The mathematical description of the 303-304-316-305 quadrangle will thus influence the updating process in a determinant way. It must be kept in mind that the use of beam elements for the modelling of these quadrangular and triangular parts is not more than a mathematical trick. For these elements, no physical interpretation must be given to the parameters that will be set by the model updating process.

The rest of the structure is characterised by a lot of holes, irregular welds and rapidly changing cross sections. A much finer mesh would be needed to model all details. The values that are applied for properties like cross sections or moments of inertia are only an approximate estimate. This model must only be used to predict the dynamic behaviour of the subframe in a global way.

The analytical resonance frequencies are shown in table 7.

Correlation.

The finite element model is coarse and the applied element properties are rough estimates. This model cannot be expected to correlate closely with the experimental data.

Table 7 evaluates the correlation by means of resonance frequency differences and MAC-values. All analytical resonance frequencies are too high. Since the difference between the analytical global mass (12.4 kg) and the real mass of the subframe (12.1 kg) is sufficiently small, the structure was modelled too stiff. The MAC-values are reasonably good for such a coarse model. MAC-values above 80% are acceptable. MAC-values above 90% are good. In order to have a reliable model, the resonance frequency differences should be less than 5% and MAC-values should exceed 80%. It does not make sense to require smaller resonance frequency differences or higher MAC-values, because the experimental resonance frequencies and mode shapes are not absolutely accurate.

Figure 20 and 21 show typical superimposed experimental and analytical receptances. The correspondence between the experimental and analytical receptances is obviously too poor.

The conclusion of the correlation study is that the finite element model of the subframe must be corrected.

Selection of updating parameters.

58 updating parameters are selected. The updating parameters are all geometric parameters that describe the stiffness and mass distribution over the structure (for instance cross area sections and area moments of inertia). The symmetry of the structure is respected.

Correction of the model.

The minimisation of the indirect receptance difference (RADSER updating method) can be combined with the minimisation of other residues. For the updating of the finite element model of the VOLVO subframe, a combination of the indirect receptance difference with the resonance frequency differences was chosen. The experimental resonance frequencies are a reasonably accurate global measure. The extra computational cost for the minimisation of the resonance frequency differences is relatively low.

For the minimisation of the indirect receptance difference, updating frequencies must be selected. Figures 22 (reference 316 (+z)) and 23 (reference 408 (-y)) and table 8 give an overview of the selected updating frequencies. Following considerations led to this selection:

- *Information content*: The updating frequencies are well distributed over the frequency range of interest. For both sets of receptances, the number of updating frequencies exceeds the number of modes in the frequency range of interest. As explained in ref. 1, the quality of the selection can be checked by a singular value decomposition of the matrix formed by the receptances for all degrees of freedom (column dimension) at all selected updaing frequencies (row dimension). This matrix is called the reference receptances matrix.Table 8 shows the relative singular values of the reference receptances matrices for both excitation points. For excitation point 316 (+z), there is one dominant singular vector, followed by three singular vectors of about equal importance (relative singular value about 0.2) and again two singular values of about equal importance (relative singular value about 0.1). The rest of the singular vectors are of less importance. This is in agreement with the fact that the frequency range of interest contains six modes. Obviously, one mode is dominantly present in the reference receptances matrix (probably the first mode) and two modes are somewhat less clear in this reference set. For reasons of stability, no updating frequencies were chosen close to the fourth and the sixth mode. These are probably the modes that are less present in the receptance references matrix. For excitation point 408 (-y), only five relative singular values of importance are found. It was already mentioned that the fifth mode was hardly excited by this excitation point. Probably, barely any information about the fifth mode is present in the receptances with 408 (-y) as reference. Thus ,the reference receptances matrix covers the available information quite well.

- *Accuracy*: All updating frequencies are selected in frequency ranges where the accuracy of the experimental receptances is believed to be sufficient.

- *Damping*: The structure exhibits low damping. An undamped finite element model was used. The updating frequencies are not selected too close to the resonance frequencies where the receptances are relatively more influenced by damping.

- *Stability*: In ref. 1 it is mentioned that for lowly damped structures, frequencies that possibly coincide with an analytical resonance frequency during the updating process must be avoided in the selection of updating frequencies. This is the reason why no updating frequencies are chosen close to the fourth and sixth experimental resonance peak. The peak of respectively the third and the fifth analytical resonance will pass the fourth and sixth experimental resonance while they converge to their corresponding experimental resonance.

With these updating frequencies, a first updating iteration is run. This first iteration already yields quite improved correlation measures (table 9) The resonance frequency differences are all less than 4% and the MAC-values globally improved.

After this first iteration, the restrictions for the updating frequencies concerning the numerical stability of the updating process are not longer valid. Updating frequencies close to the fourth and sixth experimental resonance can be selected without the risk of numerical instability. New updating frequencies are chosen in order to improve the balance of the reference receptance matrices. Figure 24 and 25 and table 10 show the updating frequencies that are selected with consideration of the accuracy, damping and stability criteria.

For excitation point 316 (+z), the relative singular values do not improve much. For excitation point 408 (-y), however, the new selection of updating frequencies yields quite some improvement (table 10).

With these updating frequencies, ten updating iterations are run. Table 11 shows the resulting frequency differences and MAC-values.

All resonance frequency differences are less than 4%. For the first four modes the MAC-values exceed 92%. The fifth mode has a MAC-value of almost 85%; which still is more than acceptable. The MAC-value of the sixth mode decreased to 72%. Normally, this MAC-value should exceed 80% to be acceptable. However, the experimental receptances hardly contained information about this mode. So it could be expected that the updating process focuses on the improvement of those modes that are best covered by the experimental receptances. Moreover, the sixth experimental mode shape looks rather noisy. This can, possibly, cause a somewhat lower MAC-value too. Figure 26 and 27 show typical superimposed experimental, original analytical and updated receptances. Much of improvement can be seen with respect to the original analytical receptances. It is the author's opinion that a better agreement must not be expected because of the high degree of idealisation of the finite element model and the limited accuracy of the experimental receptances.

On basis of the modal parameters and the comparison of experimental and analytical receptances, the conclusion is that the updated finite model is much more reliable than the original model and that it is valid for use in the frequency range from 0 to 300 Hz. If this range is limited to the first four modes, the correlation with the experimental model is even very good.

Conclusion.

In this case study, the RADSER updating technique was used to correct a very coarse finite element model of a subframe of a Volvo 480. Starting from not extremely accurate and even somewhat noisy measurements and via selections of updating parameters and updating frequencies based on simple rules of thumb and common sense, the updating process gave reliability to a coarse, and thus cheap, finite element model. Although the results of the updating of such a coarse model must be used with some reserve, this case study showed that the RADSER updating technique is useful tool in the design of mechanical structures. Coarse finite element models that are normally seen as unreliable, can be validated by means of an easy to use model updating technique.

SUMMARY.

This paper presented two case studies of FRF based model updating.

In the first application the axial stiffness and damping of rubber mounts was succesfully identified.

In the second case study, a coarse finite element model of a car subframe was validated.

These succesful applications show the validity of the presented updating technique for the verification and correction of dynamic finite element models.

REFERENCES.

1. Lammens S., Brughmans M., Leuridan J., "Updating of dynamic finite element models based on experimental receptances and the reduced analytical dynamic stiffness matrix.", to be presented at 1995 SAE Noise & Vibration Conference, Traverse City, Michigan, 1995.

2. CADA-X Modal Analysis User's Manual, LMS International, Leuven, Belgium.

3. MSC/NASTRAN User's Manual, Version 66, The MacNeal-Schwendler Corporation, Los Angeles, CA, November 1988.

Aquisition parameter	Value or option
Signal type	bandlimited noise
Frequency range source	0 Hz to 256 Hz
Length burst	80%
Sampling frequency	512 Hz
Filter cutoff	204 Hz
Blocksize	4096
Frequency range processing	0 Hz to 256 Hz
Number of averages	40
Input window	uniform
Response window	uniform
Measurement function	FRF Hv

Table 1: Aquisition parameters.

Stiffnesses (both models) (N/m)		Viscous damp. (model 1) (Ns/m)		Structural damp. (model 2)	
k_1	2.50 10^7	c_1	5	η_1	0.01
k_2	3.75 10^6	c_2	10	η_2	0.02
k_3	5.00 10^6	c_3	1000	η_3	0.50

Table 2: Original stiffness and damping parameters.

Acquisition parameter	Value or Option
Signal type	band limited noise
Frequency range source	0 Hz to 512 Hz
Length burst	60%
Sampling frequency	1024 Hz
Filter cut-off	410 Hz
Processing parameter	**Value or Option**
Block size	2048
Frequency range processing	0 Hz to 512 Hz
Number of averages	40
Input window	uniform
Response window	uniform
Measurement function	FRF Hv

Table 3: Acquisition and signal processing parameters.

Mode number	Frequency (Hz)	Damp. ratio (%)
1	77.4	0.38
2	136.0	0.14
3	166.3	0.24
4	178.2	0.43
5	271.3	0.52
6	291.2	0.33

Table 4: Overview of experimental modal parameters.

i	*Mode participation factors*			*Weighted mode complexity*	
	ref. 316: +z (%)	*ref. 408: -y (%)*	*both inputs*	*ref. 316: +z (%)*	*ref. 408: -y (%)*
1	*100.0*	*14.0*	*48.1*	*100*	*100*
2	*45.7*	*100.0*	*17.9*	*100*	*100*
3	*100.0*	*53.1*	*9.1*	*100*	*100*
4	*94.5*	*100.0*	*19.9*	*100*	*100*
5	*100.0*	*5.4*	*3.3*	*100*	*0*
6	*64.4*	*100.0*	*1.7*	*100*	*100*
all	*64.6*	*35.4*	*100.0*		

Table 5: Mode participation factors and weighted mode complexity for mode i.

	1	*2*	*3*	*4*	*5*	*6*
1	*100*					
2	*2.6*	*100*				
3	*0.1*	*0.0*	*100*			
4	*0.0*	*0.0*	*4.0*	*100*		
5	*0.1*	*0.0*	*1.5*	*0.5*	*100*	
6	*0.2*	*0.6*	*0.1*	*0.0*	*0.1*	*100*

Table 6: MAC-values (%).

Exp. mode	Exp. freq. (Hz)	Anal. mode	Anal. freq. (Hz)	Freq. diff. (%)	MAC-value (%)
1	77.4	1	95.9	23.9	95.7
2	136.0	2	150.2	10.5	94.1
3	166.3	3	198.8	19.5	87.2
4	178.2	4	201.5	13.1	62.5
5	271.3	5	299.0	10.2	66.5
6	291.2	6	347.3	19.2	83.6

Table 7: Resonance frequency differences and MAC-values.

i	ref. 316 (+z)		ref. 408 (-y)	
	f_i (Hz)	σ_i/σ_1	f_i (Hz)	σ_i/σ_1
1	65.5	1.000	70.5	1.000
2	70.5	0.277	74.0	0.697
3	72.5	0.209	124.5	0.544
4	131.0	0.178	131.0	0.290
5	133.0	0.106	133.0	0.118
6	160.0	0.087	163.0	0.026
7	162.0	0.031	309.5	0.016
8	164.0	0.018	310.5	0.007
9	263.0	0.008	312.0	0.002
10	267.0	0.004		
11	268.0	0.003		
12	308.5	0.002		
13	312.0	0.001		

Table 8: Updating frequencies and relative singular values of the reference receptances matrix.

Exp. mode	Exp. freq. (Hz)	Anal. mode	Anal. freq. (Hz)	Freq. diff. (%)	MAC-value (%)
1	77.4	1	74.4	-3.5	95.5
2	136.0	2	132.5	-2.5	94.0
3	166.3	3	166.1	-0.1	90.0
4	178.2	4	176.7	-0.8	69.8
5	271.3	5	264.9	-2.4	67.9
6	291.2	6	284.4	-2.4	84.5

Table 9: Resonance frequency differences and MAC-values.

i	ref. 316 (+z)		ref. 408 (-y)	
	f_i (Hz)	σ_i/σ_1	f_i (Hz)	σ_i/σ_1
1	65.5	1.000	66.5	1.000
2	69.5	0.397	72.5	0.755
3	72.5	0.209	82.0	0.637
4	82.0	0.140	119.5	0.477
5	86.5	0.112	128.0	0.431
6	93.5	0.107	131.0	0.221
7	126.0	0.066	140.5	0.046
8	131.0	0.027	145.5	0.012
9	140.5	0.013	162.0	0.010
10	141.5	0.008	163.0	0.008
11	160.0	0.007	183.0	0.007
12	161.0	0.006	190.0	0.005
13	163.0	0.004	307.5	0.003
14	182.0	0.004	309.5	0.003
15	185.0	0.003		
16	190.0	0.003		
17	274.5	0.002		
18	276.5	0.002		
19	294.0	0.001		
20	305.5	0.001		
21	310.5	0.001		

Table 10: Updating frequencies and relative singular values of the reference receptances matrix.

Exp. mode	Exp. freq. (Hz)	Anal. mode	Anal. freq. (Hz)	Freq. diff. (%)	MAC-value (%)
1	77.4	1	76.7	-1.0	95.3
2	136.0	2	140.9	3.6	92.1
3	166.3	3	170.3	2.4	93.3
4	178.2	4	180.0	1.0	94.5
5	271.3	5	272.7	0.5	84.9
6	291.2	6	318.3	2.1	72.4

Table 11: Resonance frequency differences and MAC-values after the updating.

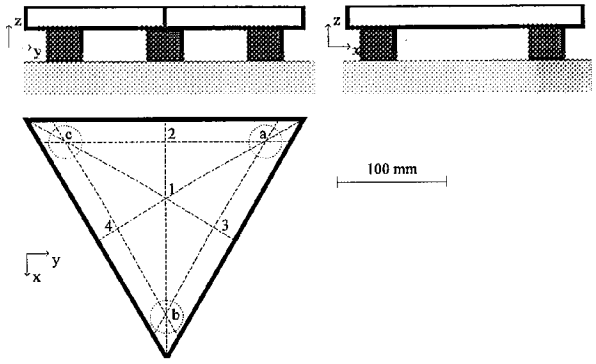

Figure 1: Set up for the identification of the mounts.

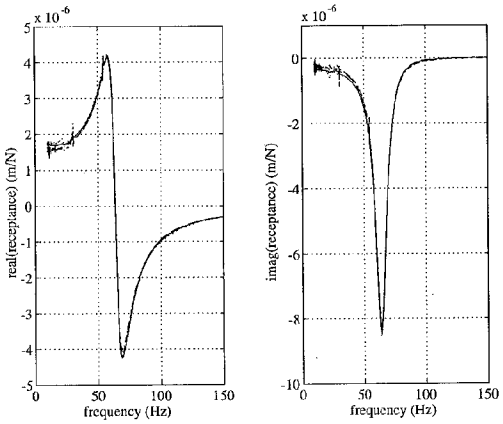

Figure 3: Experimental receptances (point 1: full line; point 2: dash-dot line; point 3: dashed line; point 4: dotted line).

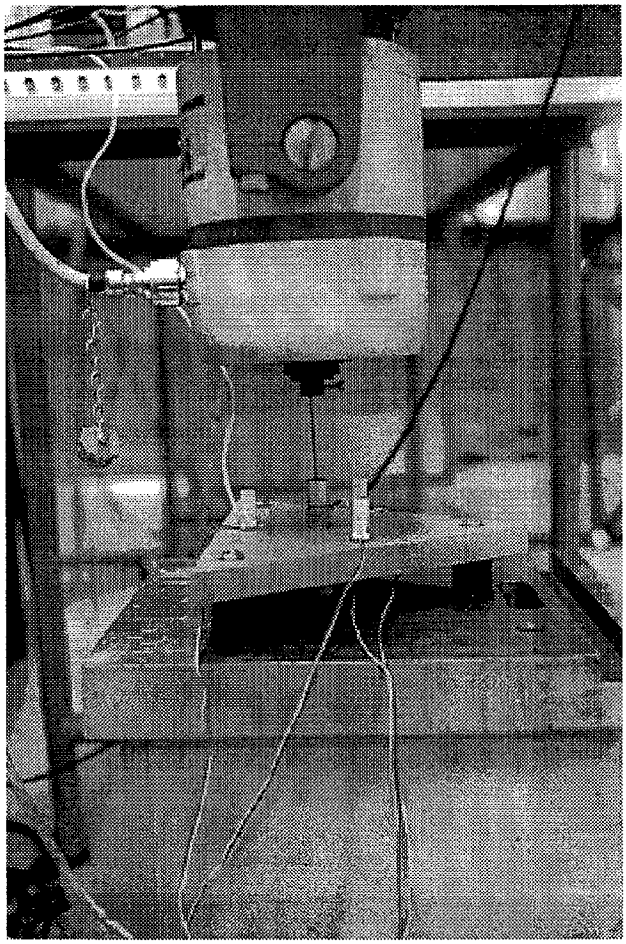

Figure 2: Experimental set up.

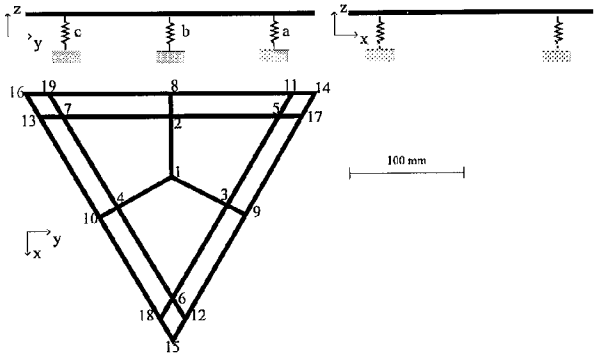

Figure 4: Finite element model.

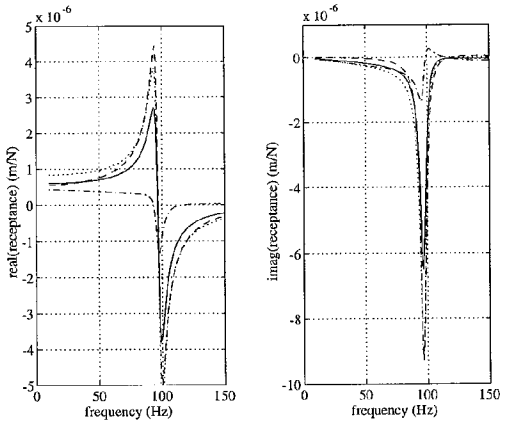

Figure 5: Superimposed analytical receptances for the viscous damping model (point 1: full line; point 2: dash-dot line; point 3: dashed line; point 4: dotted line).

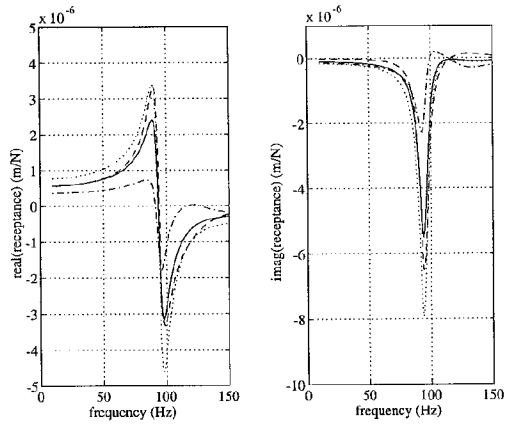

Figure 6: Superimposed analytical receptances for the structural damping model (point 1: full line; point 2: dash-dot line; point 3: dashed line; point 4: dotted line).

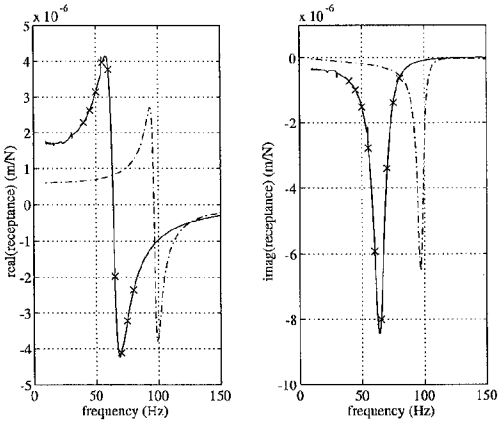

Figure 7: Experimental receptance (full line) and analytical (viscous damping) receptance (dashed line) for response at the center of the triangle and the updating frequencies (×).

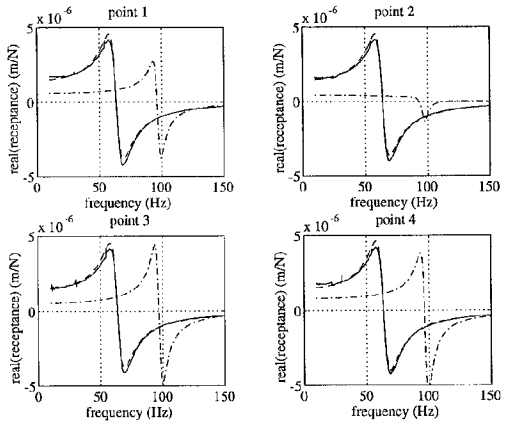

Figure 8: Real part of the experimental (full line), the original analytical (dash-dot line) and the updated analytical receptances (dashed line) for the viscous damping model.

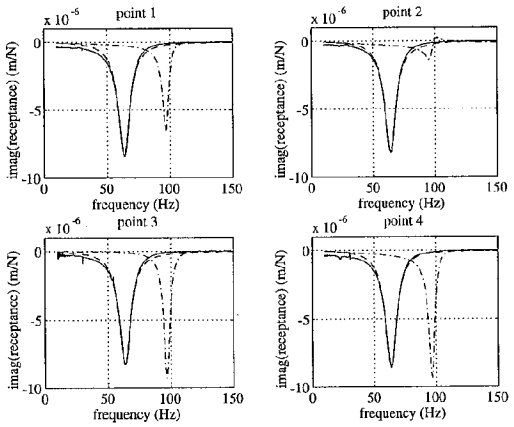

Figure 9: Imaginary part of the experimental (full line), the original analytical (dash-dot line) and the updated analytical receptances (dashed line)for the viscous damping model.

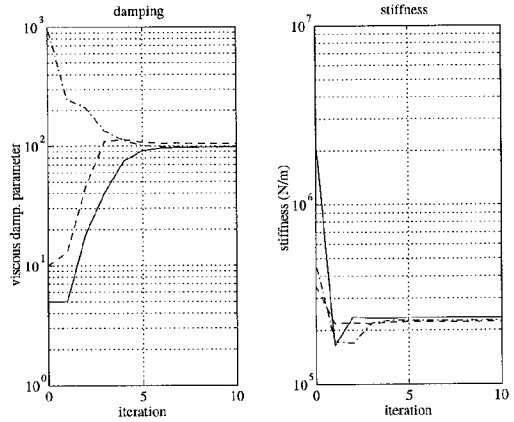

Figure 10: Convergence of the damping and stiffness parameters for the viscous damping model (mount a: full line; mount b: dashed line; mount c: dash-dot line).

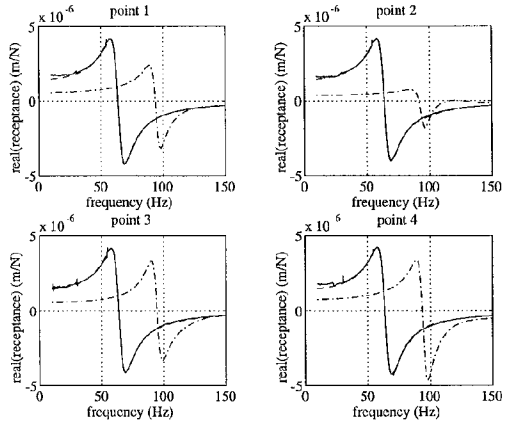

Figure 11: Real part of the experimental (full line), the original analytical (dash-dot line) and the updated analytical receptances (dashed line) for the structural damping model.

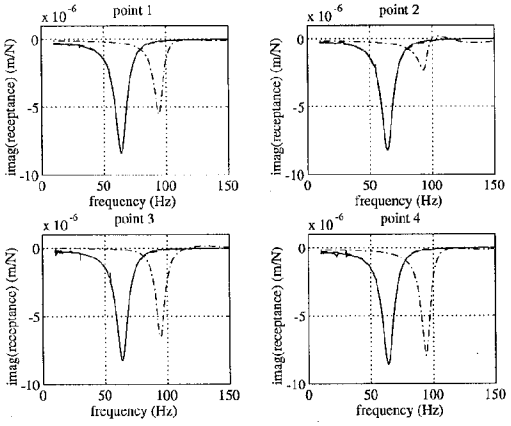

Figure 12: Imaginary part of the experimental (full line), the original analytical (dash-dot line) and the updated analytical receptances (dashed line)for the structural damping model.

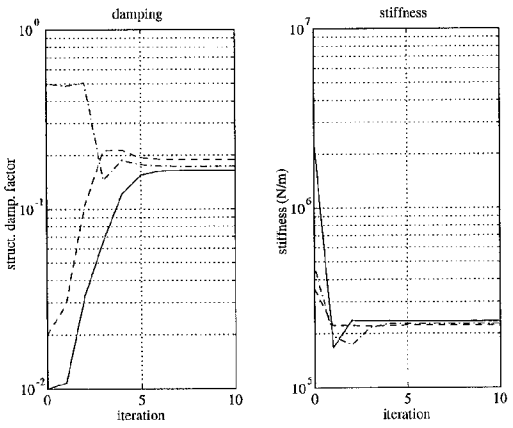

Figure 13: Convergence of the damping and stiffness parameters for the structural damping model (mount a: full line; mount b: dashed line; mount c: dash-dot line).

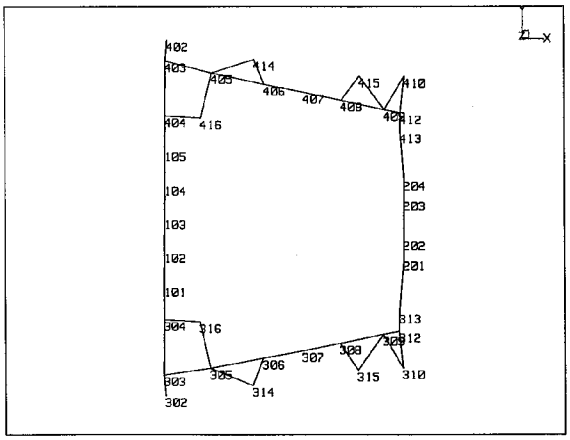

Figure 15: Measurement geometry.

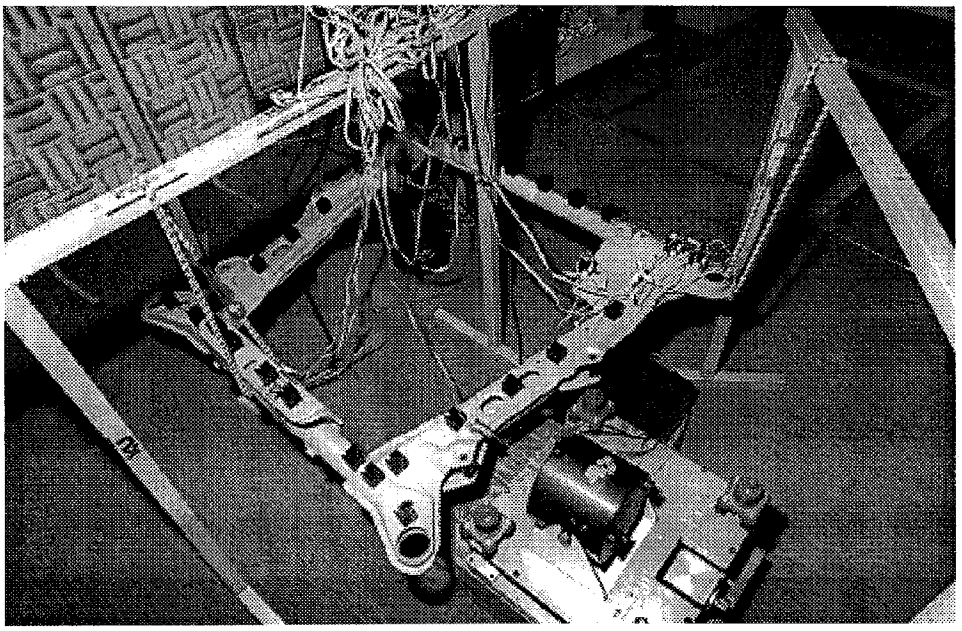

Figure 14: The subframe in the set up for the experimental modal analysis test.

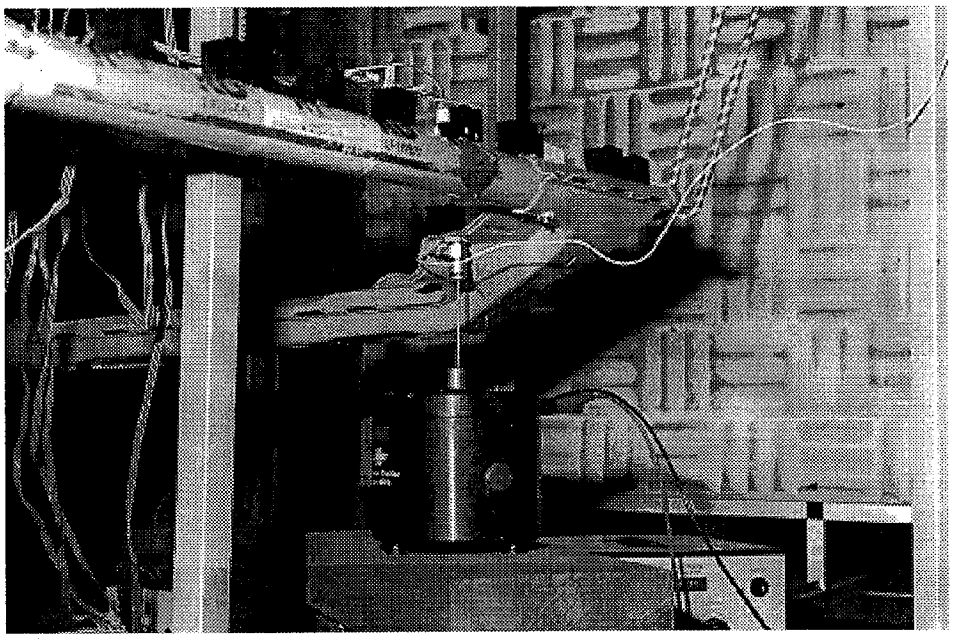

Figure 16: First excitation point.

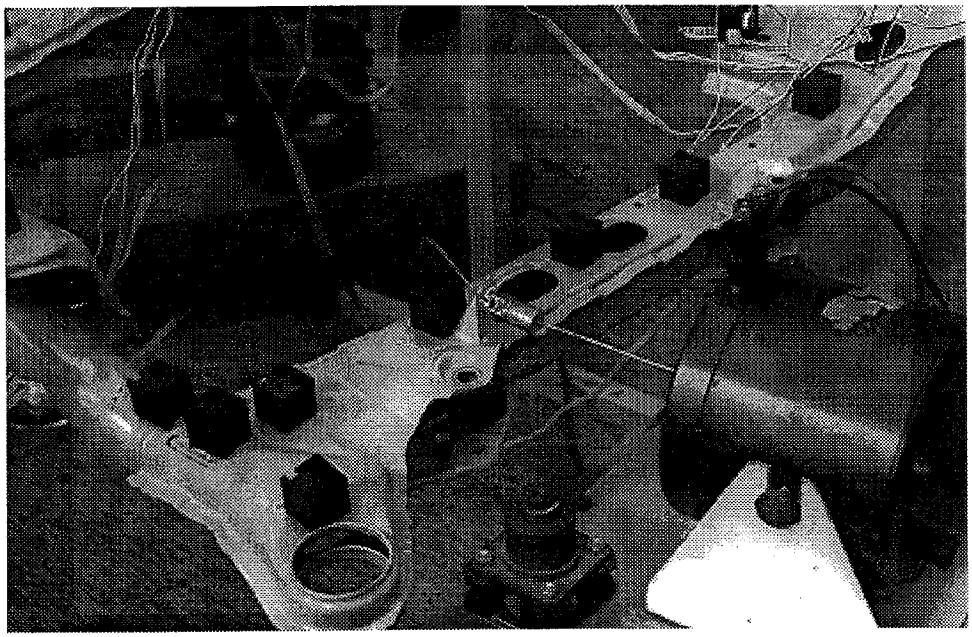

Figure 17: Second excitation point.

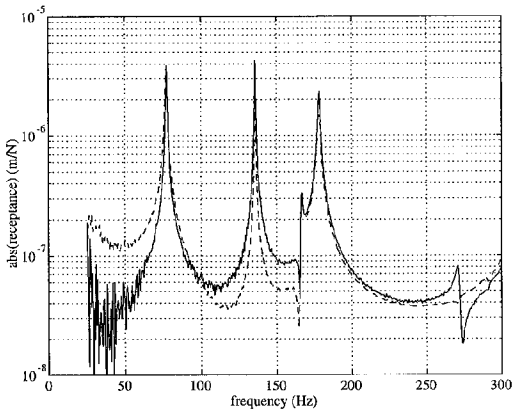

Figure 18: Reciprocity check. Full line: receptance; input: 316 (z); response: 408 (-y). Dashed line: receptance; input: 408 (-y); response: 316 (z)

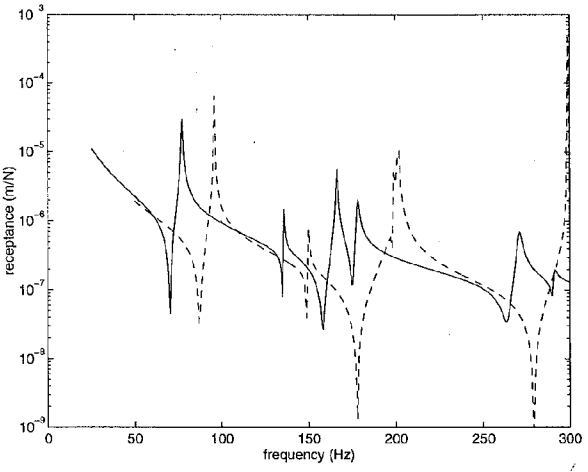

Figure 20: Experimental (full line) and analytical (dashed line) receptance; reference 316(+z), response 101(+z).

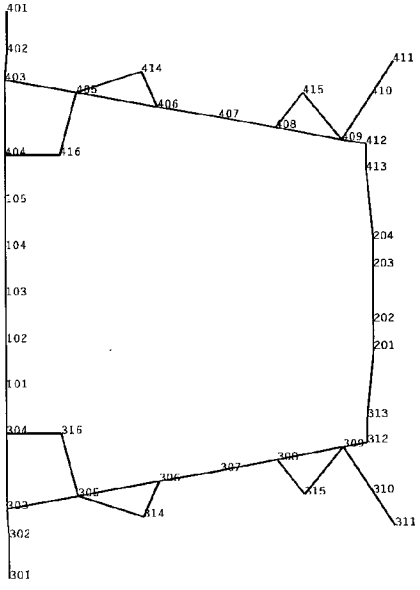

Figure 19: Finite element model of the subframe with node numbers.

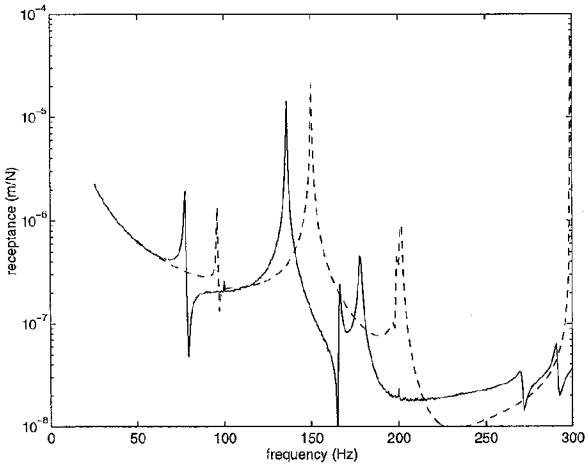

Figure 21: Experimental (full line) and analytical (dashed line) receptance; reference 408(-y), response 101(+y).

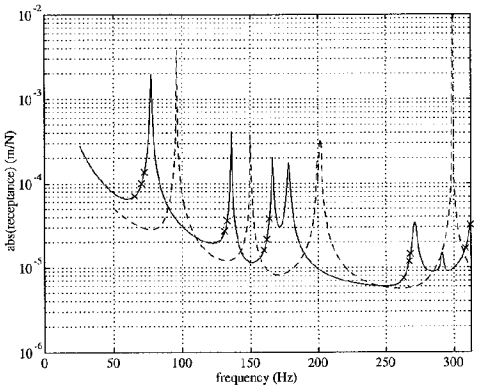

Figure 22: Sum of absolute values of the experimental (full line) and analytical (dashed line) receptances for ref.: 316 (+z), with the updating frequencies (×).

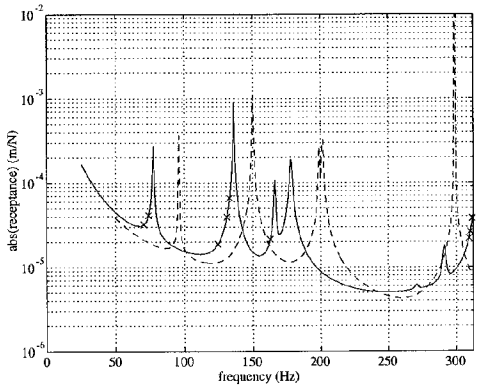

Figure 23: Sum of absolute values of the experimental (full line) and analytical (dashed line) receptances for ref.: 408 (-y), with the updating frequencies (×).

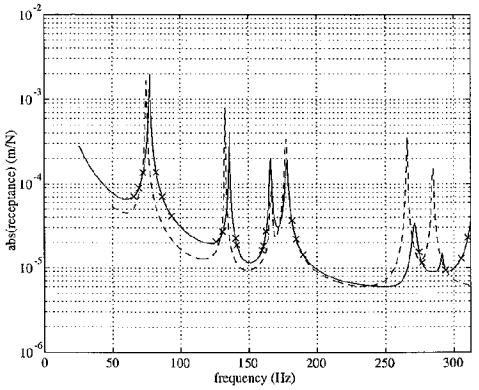

Figure 24: Sum of absolute values of the experimental (full line) and analytical (dashed line) receptances for ref.: 316 (+z), with the second selection of updating frequencies (×).

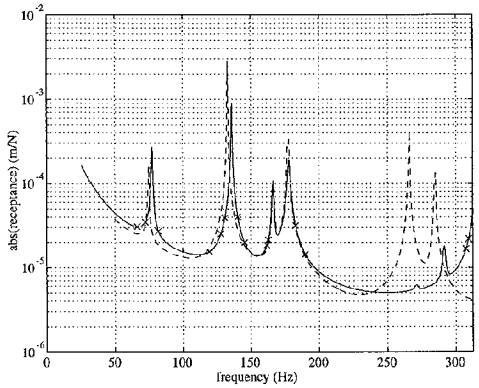

Figure 25: Sum of absolute values of the experimental (full line) and analytical (dashed line) receptances for ref.: 408 (-y), with the second selection of updating frequencies (×).

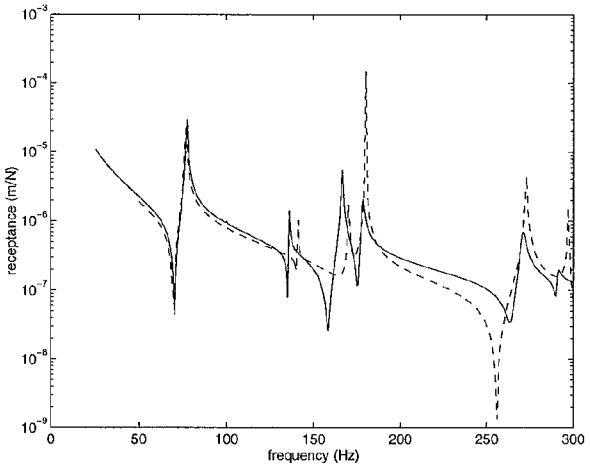

Figure 26: Experimental (full line) and analytical (dashed line) receptance; reference 316(+z), response 101(+z).

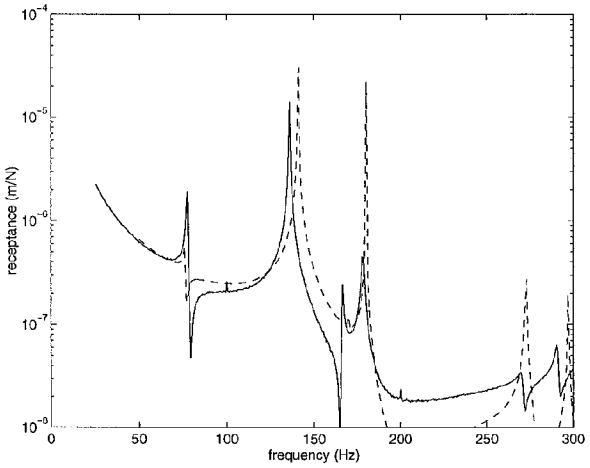

Figure 27: Experimental (full line) and analytical (dashed line) receptance; reference 408(-y), response 101(+y).